CONTRIBUTED PAPER

3-D Rat Brain Phantom for High-Resolution Molecular Imaging

Experimental studies aimed at advancing understanding of human brain disease and malfunction, and of behavior problems, may be aided by computer models of small laboratory animals.

By Frederik Johannes Beekman, *Senior Member IEEE*, Brendan Vastenhouw, Gijs van der Wilt, Marcia Vervloet, Renée Visscher, Jan Booij, Mirjam Gerrits, Changguo Ji, Ruud Ramakers, and Frans van der Have

ABSTRACT | With the steadily improving resolution of novel small-animal single photon emission computed tomography (SPECT) and positron emission tomography devices, highly detailed phantoms are required for testing and optimizing these systems. We present a three-dimensional (3-D) digital and physical phantom pair to represent, e.g., cerebral blood flow, glucose metabolism, or neuroreceptor binding in small regions of the rat brain. The anatomical structures are based on digital photographs of the uncut part of a rat brain cryosection block. The photographs have been segmented into ventricles and gray and white matter and have been stacked afterwards. In the resulting voxelized digital phantom, tracer concentration in gray and white matter can be scaled independently. This is of relevance since, e.g., cerebral blood flow or metabolism are much higher in gray than in white matter. The physical phantom is based on the digital phantom and has been manufactured out of hardened polymer using rapid prototyping, a process in which complicated 3-D objects can be built up layer by layer. X-ray computed tomography and high-resolution SPECT images of the physical phantom are compared with the digital phantom. The detailed physical phantom can be filled bubble-free. Excellent correspondence is shown between details in the digital and physical phantom. Therefore, this newly developed brain phantom will enable the optimization of high-resolution imaging for recovery of complex shaped molecular distributions.

KEYWORDS | Mouse; phantom; positron emission tomography (PET); rapid prototyping; rat; single photon emission computed tomography (SPECT); small-animal imaging; X-ray computed tomography (CT)

I. INTRODUCTION

Small laboratory animals such as rats and mice are the most widely used animals for experimental studies in neuroscience. In these animals, regional molecular aspects of behavior or disease can be studied with the aid of a wide range of in-vitro methods, including autoradiography and immunohistochemistry. These procedures require sacrificing the animal after which tissue is sliced, which can be very labor intensive. Another drawback of these in-vitro studies is that repeated studies within the same groups of animals cannot be performed, which often results in the requirement to sacrifice relatively large numbers of animals to reliably quantify dynamic processes. Furthermore, obtaining three-dimensional (3-D) digital images from two-dimensional (2-D) images of tissue slices is

Manuscript received March 9, 2009; revised June 4, 2009. First published October 6, 2009; current version published November 18, 2009.
F. J. Beekman, **B. Vastenhouw**, and **F. van der Have** are with the Image Sciences Institute, University Medical Center Utrecht, 3584 CG Utrecht, The Netherlands; with the Rudolf Magnus Institute, University Medical Center Utrecht, 3584 CG Utrecht, The Netherlands; with MILabs B.V., 3584 CX Utrecht, The Netherlands; and with Department R3, Section RD&M, Delft University of Technology, 2629 JB Delft, The Netherlands (e-mail: f.j.beekman@tudelft.nl; b.vastenhouw@tudelft.nl; brendan@isi.uu.nl; f.vanderhave@tudelft.nl).
G. van der Wilt is with Vanderwilt Techniques, 5281 LB Boxtel, The Netherlands (e-mail: g.vanderwilt@wxs.nl).
M. Vervloet, **R. Visscher**, **C. Ji**, and **R. Ramakers** are with the Image Sciences Institute, University Medical Center Utrecht, 3584 CG Utrecht, The Netherlands, and also with the Rudolf Magnus Institute, University Medical Center Utrecht, 3584 CG Utrecht, The Netherlands (e-mail: m.vervloet@nivel.nl; r.visscher@itds.nl; c.ji@umcutrecht.nl; r.m.ramakers-2@umcutrecht.nl; ruud@milabs.com).
J. Booij is with the Department of Nuclear Medicine, Academic Medical Centre, University of Amsterdam, 1105 AZ Amsterdam, The Netherlands (e-mail: j.booij@amc.uva.nl).
M. Gerrits is with the Rudolf Magnus Institute, University Medical Center Utrecht, 3584 CG Utrecht, The Netherlands (e-mail: m.a.f.m.gerrits-5@umcutrecht.nl).

Digital Object Identifier: 10.1109/JPROC.2009.2028363

extremely tedious work. Stacking of slice-images requires advanced image processing to deal with tissue cracks and other tissue deformations that often result from cryosectioning. Despite progress made in image processing for combining histological or immunohistochemical slices [1]–[3], recovering 3-D digital images from slice images cannot be performed automatically and remains extremely labor intensive.

Knowledge of the 3-D distribution of marker molecules offers the possibility to quantify processes in 3-D structures of the brain like, e.g., "How much perfusion is there in gray matter in the left medial temporal lobe?" or "How many molecules and associated receptors are present in the right and left olfactory tubercle?" Over the last decade, many groups have started to study the brain in small laboratory animals using molecular imaging methods such as high-resolution small-animal single photon emission computed tomography (SPECT) and positron emission tomography (PET). These techniques enable one to obtain the 3-D distribution of radiolabeled molecules (radiotracers or radiopharmaceuticals) in vivo [4]–[18]. This offers the unique possibility to perform repeated studies within the same groups of animals, which is not possible with immunohistochemistry.

New scanners and systems under development can be tested using simulated scans and digital brain phantoms (e.g., [19]–[21]). This is extremely valuable. However, simulations are limited in their accuracy, in particular to model differences between individual scanners. For many years, physical phantoms representing human brain structures that can be filled with contrast agents or radiotracers have played an important role in experimentally validating clinical imaging systems such as SPECT, PET, X-ray computed tomography (CT), and magnetic resonance imaging [22].[1] For example, brain areas that express specific receptors (e.g., the striatum with high concentrations of dopamine D_2 receptors or dopamine transporters) can be evaluated [23], [24]. Several miniature phantoms with mathematical shapes, e.g., tiny resolution phantoms [25]–[27] and Defrise phantoms for testing sampling capabilities (e.g., [21], [25], [28]), are available for high-resolution imaging in small laboratory animal modalities. Phantoms with much more complex anatomical shapes can be useful to estimate how much detail can be visualized in specific types of small-animal studies, to compare and improve imaging systems for specific imaging tasks, and to improve acquisition and reconstruction parameters or to test image registration algorithms. Moreover, it may be of value to evaluate different concentrations of contrast agents or radioactivity.

Digital and physical phantoms can also be used to estimate the performance of small-animal imaging systems for a variety of imaging tasks. Simulations with digital phantoms permit controlled evaluation over a wide range of conditions (e.g., different tracer concentration, isotopes emitting different energy photons, different acquisition times, artifacts, different lesion sizes, lesion position, or geometric distortions). Such simulations have become increasingly important with the rapid growth of the number of small-animal SPECT and PET imaging systems, i.e., for analysis of brain cell metabolism and regional brain perfusion. Next to digital phantoms, physical phantoms are important since i) not all aspects of imaging systems are covered by a simulation model and ii) simulation cannot replace an experimental test of a specific system. With physical phantoms, in contrast to imaging living animals, stable and perfectly reproducible known tracer distributions can be created. Since the spatial resolution of small-animal SPECT and PET devices is rapidly improving, phantoms with increasing levels of detail are required, including phantoms containing small anatomical details. Although digital rat 3-D brain atlases have been produced [29]–[31], to our knowledge no detailed 3-D physical rat brain phantom has been manufactured so far. The availability of such a phantom is important since the rat may often be the animal of choice in experimental neuroscience since a huge body of molecular, anatomical, behavioral, and electrophysiological data from rats already exists.

Recently, we developed SPECT imaging devices with sub-half-millimeter resolution (U-SPECT [26], [27], [32]–[34]). In addition, PET devices are being developed that can obtain resolutions below 1 mm [35]–[37]. The goal of this paper is to present a physical rat brain phantom and its finely voxelized digital version that facilitate testing and optimizing of these high-resolution devices developed for imaging small laboratory animals. We briefly explain how the anatomical shape of the digital phantom has been obtained, how the physical phantom has been manufactured, and how it can be filled with tracers and contrast agents. Lastly, ultra-high-resolution SPECT images will be presented together with X-ray CT images as an initial validation of this prototype phantom.

II. METHODS

A. Obtaining Brain Shape and Gray/White Matter Structure

The following procedure was performed to obtain anatomical structures of gray and white matter: an adult, male Wistar rat weighing 275 g was decapitated under anesthesia. The brain was removed and frozen quickly. Subsequently, 20-μm-thick coronal slices of the brain were removed using a cryostat. Each time after removing 100 μm of tissue, photographs (with a resolution of 2000 $\times$ 1312 pixels) of the uncut block face were acquired with a Nikon D1x digital camera. The camera was mounted onto a heavy tripod standing on the floor close to the cryostat.

The photographs were segmented into gray matter, white matter, and ventricles. Furthermore, the outline of

[1]http://www.rsdphantoms.com/.

the brain was segmented. The segmentation (see Fig. 1) was performed semiautomatically using the graphical software package Gimp (GNU Image Manipulation Program, www.gimp.org). The "magic wand" tool was used to select a contiguous region with a fixed threshold starting from the pixels with a specified color. The edges of the selection are then refined by a small adjustment to the radius of the boundaries such that the edges are smooth and show no discontinuities. Afterwards, the white matter structures segmented from the photos were verified using the rat brain atlas from Paxinos and Watson [29]. The number of segmented structures as well as their shape was compared with those present in the atlas. In this way, no structures were omitted from the segmentation. The structures in a specific slice were also compared to the adjacent slices to make sure no large discontinuities are introduced. Lastly, the slices were stacked and a median filter was used to remove ripples in the axial direction.

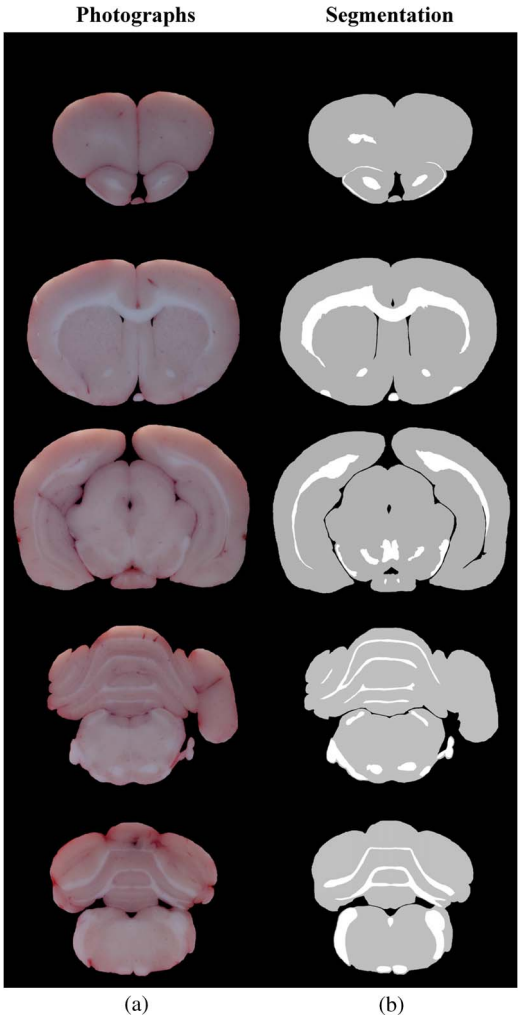

Fig. 1. *(a) Selection of photographs taken from the uncut block of rat brain with fixed camera, with the outline already segmented. (b) Corresponding slices of segmented rat brain.*

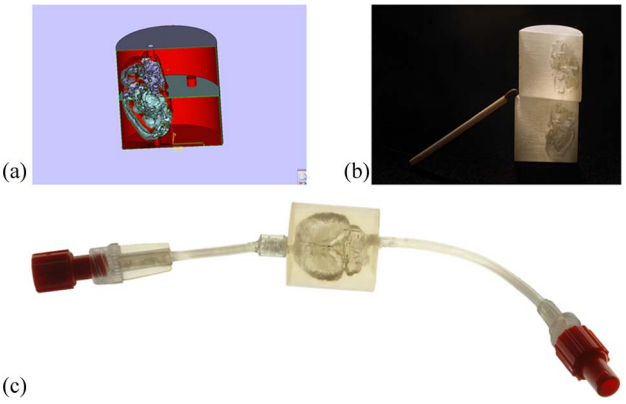

Fig. 2. *(a) 3-D representation of the phantom. (b) Cross-section of the phantom. (c) Polished phantom with tubes and connectors for luer lock valves.*

B. Manufacturing of the Physical Phantom

A cylinder with a diameter of 23 mm is used to represent the rat head in which a cavity representing the gray matter is created that can be filled with a tracer or contrast agent. The gray matter shape was obtained from the voxelized digital brain phantom by isosurface generation. This phantom is converted to STL file format, which approximates the shape of the phantom by a large number of small triangular facets. The size of the each facet depends on the local curvature of the contour, since strong curvature can only be modeled by a higher number of smaller facets. The STL file was then used by the rapid prototyping machine.

The 3-D model was then "cut" into thin horizontal slices of 0.036 mm and transferred to a stereolithography machine that uses a computer-controlled laser to draw the bottom cross-section onto the surface of the liquid polymer (Fullcure 720, density 1.092 g/ml). The polymer hardens, where it is irradiated by the laser beam. Then the phantom is lowered by 0.036 mm and subsequently the next cross-section is drawn directly on top of the previous layer. This is repeated until the entire volume is finished. In the bottom and top layers, holes are incorporated for the mounting of tubes with luer lock connectors, which are used for mounting of three-way valves and syringes for filling the phantom. After removing the phantom from the liquid polymer, the compartment is flushed and cured with ultraviolet. The outside was polished to monitor fluid level when filling the phantom. The physical phantom is shown in Fig. 2.

C. Filling the Phantom

$^{99\,m}$Tc-tetrofosmin and X-ray CT contrast agent were mixed to obtain a final concentration of 37 MBq/ml and 10% (dilution by volume) Iopromide (Ultravist 150). The total volume of the mixture was 4 ml. On the cerebellum side of the phantom, a three-way valve ("valve A") was connected to a luer lock adapter with a septum. On the

cerebrum side, another three-way valve ("valve B") was connected to an empty syringe. The phantom was placed in a lab stand with the cerebellum side pointing downwards. The phantom was evacuated using a vacuum pump. After 30 min of evacuation, valve A was turned and the vacuum pump disconnected.

In order to preserve the vacuum, the phantom was filled through the septum connected to valve A via a needle attached to a syringe with the radioactive mixture. This way, 1.5 ml of the liquid was transferred into the phantom. Then the phantom was closed off on this side and the septum was removed. The syringe with the mixture was directly connected to valve A and the mixture was gently flushed through the phantom several times to ensure a complete filling and remove remaining air bubbles from the phantom. The bubbles were removed from the system through valve B. Lastly, the valves were replaced by stops before the phantom was scanned.

D. Imaging of the Physical Phantom

Images of the phantom were acquired with dedicated small-animal CT and SPECT. The microSPECT device used here (U-SPECT-II, Milabs BV, The Netherlands [27]) can be equipped with differently sized cylindrical multipinhole collimators. Several easily exchangeable collimators are available, i.e., for i) whole-body and focused mouse imaging, ii) whole body and focused rat imaging, and iii) dedicated rat brain imaging. Using this prototype, a rat brain collimator with 49 0.35-mm gold pinholes, a reconstructed resolution of 0.35 mm can be obtained. The estimated sensitivity of this prototype collimator was 0.05% (390 cps/MBq) for Tc-99 m. Further details about system performance are described in [27]. A graphical user interface incorporating preselection of the field-of-view with the aid of optical images of the animal enables focusing of the pinholes to the volume of interest, thereby minimizing the scanning time and maximizing the sensitivity. The field of view was made as large as the entire head phantom by scanning the phantom through the pinhole focus area [33]. SPECT images were iteratively reconstructed using a multithreaded programmed ordered subset expectation maximization algorithm modeling the distance dependent camera and pinhole collimator response [38]. No correction for attenuation or scatter was applied for this case. In order to avoid problems with decay, dynamic scanning was applied, and reconstructions of different time frames were added to a single 3-D image. The long SPECT acquisition (10 h) was chosen here to get as much detail of the phantom content as possible, e.g., to know if the tracer gets into tiny structures or if air bubbles were removed.

The microCT used in this study (U-CT, Milabs BV, The Netherlands) is a fast cone beam CT system dedicated for high-throughput in-vivo scanning of small animals. The X-ray source is an air-cooled metalloceramic tube with a voltage range of 20–65 kV. The X-ray detector is a 1280 × 1024 pixel, 12-bit semiconductor digital camera. The scanning volume has a diameter of 82 mm and a length of 82 mm for a single circular orbit. During scanning, the source-detector assembly turns around the animal, which remains stationary in the transferable bed. The reconstructed voxel size used was 83 μm (isotropic), which is close to the resolution that can be obtained.

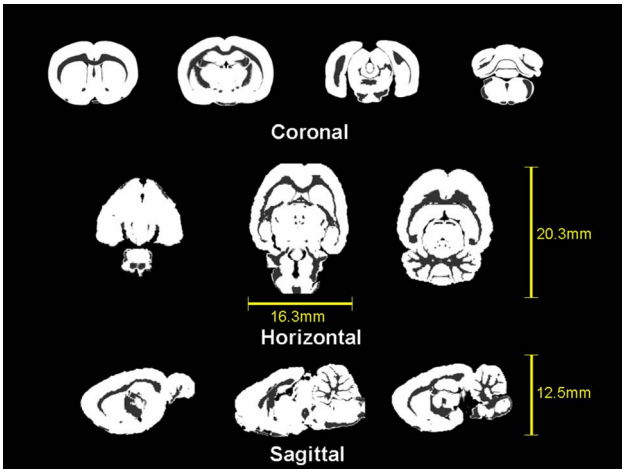

Fig. 3. *Selection of slices through digital rat brain phantom. WM : GM equals 1 : 5.*

1) Image Registration: Since the digital phantom, the X-ray CT scan and SPECT images of the phantom have sufficient mutual information to be matched to each other, and the resolution of the digital phantom and CT scan is much higher than that of the SPECT images, we used a fusion tool (PMOD Technologies, Switzerland) to find the initial transformation from SPECT images to corresponding CT images. With this initial input of transformation, we registered the SPECT image to the CT image using the normalized mutual information algorithm [39].

III. RESULTS

A. Digital Phantom

Fig. 3 shows a selection of coronal, horizontal, and sagittal slices of the phantom at a linear gray scale, assuming a white matter (WM) to gray matter (GM) concentration ratio of 1 : 5. The figures clearly show that the alignment of the individually segmented photographs is sufficiently accurate due to the stable position of the camera, application of image filtering, and corrections of possible misalignments during acquisition of the photographs.

The images show that a truly 3-D phantom was obtained. The digital version of the rat brain phantom, including a down-scaled version to mimic a mouse brain, is publicly available.[2]

[2]www.rrr.tudelft.nl/rdm ⟶ People ⟶ Freek J. Beekman ⟶ Rat & Mouse Brain Phantom.

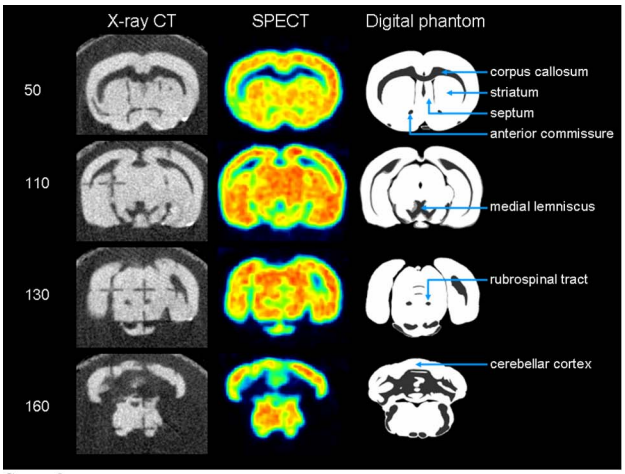

Fig. 4. ***Images of the X-ray CT scan, the SPECT scan, and the digital phantom with white matter intensity put to zero under three orthogonal directions.***

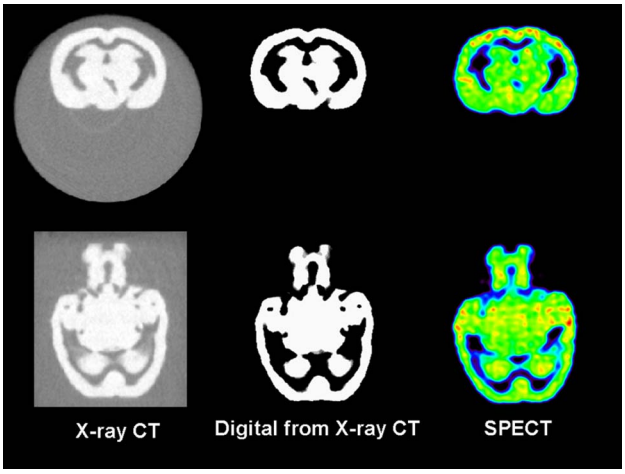

Fig. 5. ***Phantom without supporting structures, where the digital phantom is extracted from a segmented CT scan.***

B. Physical Phantom

Fig. 4 shows images taken from the (a) X-ray CT and (b) SPECT, which are compared with the digital phantom (c) with white matter intensity put to zero. The correspondence between the digital phantom and the X-ray CT and SPECT images of the physical phantom is excellent. For example, in coronal slices, the corpus callosum, striatum, septum, anterior commissure, and medial lemniscus are visible in CT and in SPECT. In the sagittal slices, the same can be said about the corpus callosum, lateral ventricle, and tiny parts of the cerebellum and striatum. The horizontal slices of SPECT and CT images clearly show the cerebellar cortex, lateral ventricles, hippocampus, striatum, and lateral ventricles. In this realization, structures that support the details of the brain anatomy are also visible, in both the CT scan and the SPECT images. These "+"-shaped structures were generated automatically by the rapid prototyping machine in the manufacturing process.

Newer physical phantoms are being developed using the latest generation rapid prototyping machines that do not require such structures (Fig. 5) but they deviate slightly from the digital phantom. In order to estimate the ground truth underlying such a phantom, one could segment the CT scan (in this case by simple $3 \times 3 \times 3$ median filtering followed by applying a threshold). Again, a long SPECT scan was acquired, i.e., (16.5) hours, in order to see as much detail as possible for validation of the phantom. The initial activity concentration was 50 MBq/ml.

IV. DISCUSSION AND CONCLUSION

We have developed methods to create highly detailed digital and physical 3-D rat brain phantoms that can be used to optimize imaging studies in rat brains. The phantom accuracy has been validated by acquisition of X-ray CT and SPECT images of the brain phantom that showed excellent correspondence with the digital phantom, which indicates that rapid prototyping may be a method that is well suited to produce such complex phantoms.

The methods to segment WM and GM from cryosections were only partly automated, and parameters needed to be adjusted slice by slice guided by for example an anatomical rat brain atlas. More advanced and automatic segmentation is possible, but this will require more regulated conditions for taking the photos. For example, i) the light conditions need to be fixed, ii) the focus plane of the lens needs to stay constant, iii) a dedicated macro lens with minimal distortion is required, and iv) the camera needs to move exactly in line with the slicing.

For emulating different tracer concentrations within patients, 3-D physical phantoms have been produced with inkjet printers [40], [41]. By stacking the 2-D radioactive prints made out of paper with layers of different materials in between, effects of attenuation and scatter can be switched on and off. A denser material, such as is used in the phantom presented here, is definitely required for PET phantom experiments in order to limit the positron range [42]. In practice, filling a phantom may be easier than printing a phantom and stacking prints and positron capturing material. Since inkjet printing of a phantom can be done in any variety of tracer concentration, both methods will have both unique and overlapping applications.

In reality, the ratio between cerebral blood flow in WM and GM is often assumed to be 1 : 5 [22]. Different WM : GM ratios can also be emulated in our digital phantom. In the present manufacturing process of the physical phantom with rapid prototyping, we did not yet mimic adjacent areas with different concentrations since walls between WM and GM would become either extremely fragile or too thick to meet our goals. As a result, we choose to only model the largest structure (GM) with the highest tracer concentration as a compartment that can be filled with a tracer. In future versions, we will try to create separate reservoirs, but the wall thickness that is required to produce these walls will result in i) removal of thin structures and ii) phantoms that are very fragile and complex. It may be of value to evaluate different concentrations of contrast agents or radioactivity for the white matter (WM) and gray matter (GM) separately. This is of relevance since not only the cerebral blood flow is much higher in GM than WM in healthy brains [43], but also glucose metabolic rates and the expression of most receptors in the brain [44], [45]. For example, the expression of serotonin-1A receptors is higher in cerebellar GM than in cerebellar WM in healthy controls [46]. On the other hand, microglia cells (the brain's intrinsic macrophages) play a major role in inflammatory processes in the brain and are much more common in WM than GM. Activated microglia cells express peripheral benzodiazepine receptors, which can be visualized with [^{11}C]PK11195 PET and [^{123}I]PK11195 SPECT [47], [48]. Activated microglia are involved in the immune response of multiple sclerosis. Indeed, in multiple sclerosis, an increase of [^{11}C]PK11195 binding in WM has been shown [48]. In other pathological conditions, it may also be of relevance to discriminate WM from GM activity. For example, as compared to controls, in schizophrenia elevated glucose activity in WM matter was most pronounced in the center of large white matter tracts, especially the frontal parts of the brain [49]. Alzheimer's disease is characterized neuropathologically by deposition of so-called amyloid plaques. Interestingly, in Alzheimer's disease the WM is relatively unaffected by amyloid deposition [50]. For that case, our phantom technology may offer the unique possibility to mimic these pathological conditions in animal models of these diseases.

For emulating phantoms that, for example, represent the dopaminergic system, division in different parts could be realized already with the technology that is presented in this paper (e.g., left and right striatum and parts of the striatum such as putamen and caudate nucleus [23]). One then needs to make separate filling channels to cavities that need to be filled with different tracer concentrations. Phantoms of different neural systems can also be derived from autoradiographs, but this is an extremely time- and labor-consuming task because of the aforementioned problem of stacking pictures of deformed tissue slices to obtain an artifact-free 3-D tracer distribution image [51], [52].

Small regions within the brain have become focal points of interest among behavioral scientists. For example, dopaminergic activity in the nucleus accumbens (ventral part of the striatum) is involved in processes related to reward, including the reinforcing effects of drugs of abuse (for a review see Berridge [53]), while the expression of several peptides in the rat paraventricular nucleus of the hypothalamus is associated with food intake, and consequently with the risk for overeating and obesity [54]. In this regard, our presently developed ultra-high-resolution phantom platform technology, which will also be used to produce next phantom versions that represent other neural structures, could be made useful for a broader range of tasks, e.g., to evaluate the accuracy to measure activity within the nucleus accumbens or in subdivisions of the hypothalamus.

The general introduction of this realistic prototype phantom as to the sizes and structures of the rat brain may finally put researchers into the position to develop a standardized procedure for the determination of scanner characteristics in specific imaging tasks, which then would be comparable at last. It would not require the use of animals, with the additional advantage that a system can be optimized outside the animal lab. ■

REFERENCES

[1] M. M. Chakravarty, G. Bertrand, C. P. Hodge, A. F. Sadikot, and D. L. Collins, "The creation of a brain atlas for image guided neurosurgery using serial histological data," *Neuroimage*, vol. 30, pp. 359–376, Jan. 2006.

[2] V. Arsigny, X. Pennec, and N. Ayache, "Polyrigid and polyaffine transformations: A novel geometrical tool to deal with non-rigid deformations—Application to the registration of histological slices," *Med. Image Anal.*, vol. 9, pp. 507–523, Dec. 2005.

[3] B. Kim, J. L. Boes, K. A. Frey, and C. R. Meyer, "Mutual information for automated unwarping of rat brain autoradiographs," *Neuroimage*, vol. 5, pp. 31–40, Jan. 1997.

[4] P. Blanckaert, I. Burvenich, S. Staelens, S. De Bruyne, L. Moerman, L. Wyffels, and

F. De Vos, "Effect of cyclosporin A administration on the biodistribution and multipinhole muSPECT imaging of [(123)I]R91150 in rodent brain," *Eur. J. Nucl. Med. Mol. Imag.*, vol. 36, pp. 446–453, Mar. 2009.

[5] D. M. Araujo, S. R. Cherry, K. J. Tatsukawa, T. Toyokuni, and H. I. Kornblum, "Deficits in striatal dopamine D(2) receptors and energy metabolism detected by in vivo microPET imaging in a rat model of Huntington's disease," *Exp. Neurol.*, vol. 166, pp. 287–297, Dec. 2000.

[6] A. H. Moore, C. L. Osteen, A. F. Chatziioannou, D. A. Hovda, and S. R. Cherry, "Quantitative assessment of longitudinal metabolic changes in vivo after traumatic brain injury in the adult rat using FDG-microPET," *J. Cereb. Blood Flow Metab.*, vol. 20, pp. 1492–1501, Oct. 2000.

[7] H. I. Kornblum, D. M. Araujo, A. J. Annala, K. J. Tatsukawa, M. E. Phelps, and S. R. Cherry, "In vivo imaging of neuronal activation and plasticity in the rat brain by high-resolution positron emission tomography (microPET)," *Nat. Biotechnol.*, vol. 18, pp. 655–660, Jun. 2000.

[8] P. D. Acton, S. R. Choi, K. Plössl, and H. F. Kung, "Quantification of dopamine transporters in the mouse brain using ultra-high resolution single-photon emission photography," *Eur. J. Nucl. Med.*, vol. 29, pp. 691–698, May 2002.

[9] Y. J. Kim, M. Ichise, J. R. Ballinger, D. Vines, S. S. Erami, T. Tatschida, and A. E. Lang, "Combination of dopamine transporter and D2 receptor SPECT in the diagnostic evaluation of PD, MSA, and PSP," *Move. Disorders*, vol. 17, pp. 303–312, 2002.

[10] L. Hongfeng, F. J. Gildehaus, S. Dresel, J. T. Patt, M. Shen, T. Zhu, B. Liu, Z. Tang, K. Tatsch, and K. Hahn, "Comparison of in vivo dopamine D2 receptor binding of [123I]AIBZM and [123I]IBZM in rat brain," *Nucl. Med. Biol.*, vol. 28, pp. 383–389, 2001.

[11] S. Nikolaus, C. Antke, K. Kley, M. Beu, A. Wirrwar, and H. W. Müller, "Pre-treatment with haloperidol reduces [^{123}I]FP-CIT binding to the dopamine transporter in the rat striatum—An in vivo imaging study with a dedicated small animal SPECT," *J. Nucl. Med.*, to be published.

[12] G. Andringa, B. Drukarch, J. G. J. M. Bol, K. de Bruin, K. Sorman, J. B. A. Habraken, and J. Booij, "Pinhole SPECT imaging of dopamine transporters correlates with dopamine transporter immunohistochemical analysis in the MPTP mouse model of Parkinson's disease," *Neuroimage*, vol. 26, pp. 1150–1158, 2005.

[13] J. Booij, K. de Bruin, J. B. A. Habraken, and P. Voorn, "Imaging of dopamine transporters in rats using high-resolution pinhole single-photon emission tomography," *Eur. J. Nucl. Med. Mol. Imag*, vol. 29, pp. 1221–1224, 2002.

[14] J. B. A. Habraken, K. de Bruin, M. Shehata, J. Booij, R. Bennink, B. L. F. van Eck Smit, and E. B. Sokole, "Evaluation of high-resolution pinhole SPECT using a small rotating animal," *J. Nucl. Med.*, vol. 42, pp. 1863–1869, Dec. 2001.

[15] S. Nikolaus, R. Larisch, A. Wirrwar, M. Jamdjeu-Nouné, C. Antke, M. Beu, N. Schramm, and H. W. Müller, "[I-123]Iodobenzamide binding to the rat dopamine D-2 receptor in competition with haloperidol and endogenous dopamine—An in vivo imaging study with a dedicated small animal SPECT," *Eur. J. Nucl. Med. Mol. Imag.*, vol. 32, pp. 1305–1310, 2005.

[16] S. Nikolaus, M. Beu, A. Wirrwar, C. Antke, and H. W. Müller, "In vivo snapshots of the dopaminergic synapse in small animals," *Mol. Psych.*, vol. 10, pp. 516–518, Jun. 2005.

[17] B. Vastenhouw, F. van der Have, A. J. A. van der Linden, L. von Oerthel, J. Booij, J. P. H. Burbach, M. P. Smidt, and F. J. Beekman, "Movies of dopamine transporter occupancy with ultra-high resolution focusing SPECT," *Mol. Psych.*, vol. 12, pp. 984–987, 2007.

[18] C. Jongen, K. de Bruin, F. J. Beekman, and J. Booij, "Pinhole SPECT imaging of D2 dopamine receptors and endogenous dopamine release in mice," *Eur. J. Nucl. Med. Mol. Imag.*, vol. 35, pp. 1692–1698, 2008.

[19] I. G. Zubal, C. R. Harrel, E. O. Smith, Z. Rattner, G. Gindi, and P. B. Hoffer, "Computerized 3-Dimensional segmended human anatomy," *Med. Phys.*, vol. 21, pp. 299–302, 1994.

[20] H. Zaidi and X. G. Xu, "Computational anthropomorphic models of the human anatomy: The path to realistic Monte Carlo modeling in radiological sciences," *Annu. Rev. Biomed. Eng.*, vol. 9, pp. 471–500, 2007.

[21] F. J. Beekman and B. Vastenhouw, "Design and simulation of a high-resolution stationary system for small animals," *Phys. Med. Biol.*, vol. 49, pp. 4579–4592, 2004.

[22] E. J. Hoffman, P. D. Cutler, W. M. Digby, and J. C. Mazziotta, "3-D phantom to simulate cerebral blood flow and metabolic images for PET," *IEEE Trans. Nucl. Sci.*, vol. 37, pp. 616–620, Apr. 1990.

[23] J. Booij, G. Tissingh, G. J. Boer, J. D. Speelman, J. C. Stoof, A. G. M. Janssen, E. C. Wolters, and E. A. van Royen, "[123I]SPECT shows a pronounced decline of striatal labelling in early and advanced Parkinson's disease," *J. Neurol. Neurosurg. Psych.*, vol. 62, pp. 133–140, 1997.

[24] N. P. Verhoeff, O. Kapucu, E. Sokole-Busemann, E. A. van Royen, and A. G. Janssen, "Estimation of dopamine D2 receptor binding potential in the striatum with iodine-123-IBZM SPECT: Technical and interobserver variability," *J. Nucl. Med.*, vol. 34, pp. 2076–2084, 1993.

[25] R. J. Jaszczak, J. Li, H. Wang, M. R. Zalutsky, and R. E. Coleman, "Pinhole collimation for ultra-high-resolution, small-field-of-view SPECT," *Phys. Med. Biol.*, vol. 39, pp. 425–437, 1994.

[26] F. J. Beekman, F. van der Have, B. Vastenhouw, A. J. A. van der Linden, P. P. van Rijk, J. P. H. Burbach, and M. P. Smidt, "U-SPECT-I: A novel system for submillimeter-resolution tomography with radiolabeled molecules in mice," *J. Nucl. Med.*, vol. 46, pp. 1194–1200, 2005.

[27] F. van der Have, B. Vastenhouw, R. M. Ramakers, W. Branderhorst, J. O. Krah, C. Ji, S. Staelens, and F. J. Beekman, "U-SPECT-II: An ultra-high-resolution device for molecular small-animal imaging," *J. Nucl. Med.*, vol. 50, pp. 599–605, 2009.

[28] S. D. Metzler, K. L. Greer, and R. J. Jaszczak, "Helical pinhole SPECT for small-animal imaging: A method for addressing sampling completeness," *IEEE Trans. Nucl. Sci.*, vol. 50, pp. 1575–1583, 2003.

[29] G. Paxinos and C. Watson, *The Rat Brain Atlas in Stereotaxic Coordinates, Compact*, 3rd ed. San Diego, CA: Academic, 1997.

[30] D. J. Rubins, W. P. Melega, G. Lacan, B. Way, A. Plenevaux, A. Luxen, and S. R. Cherry, "Development and evaluation of an automated atlas-based image analysis method for microPET studies of the rat brain," *Neuroimage*, vol. 20, pp. 2100–2118, 2003.

[31] C. Casteels, P. Vermaelen, J. Nuyts, A. Van Der Linden, V. Baekelandt, L. Mortelmans, G. Bormans, and K. Van Laere, "Construction and evaluation of multitracer small-animal PET probabilistic atlases for voxel-based functional mapping of the rat brain," *J. Nucl. Med.*, vol. 47, pp. 1858–1866, Nov. 2006.

[32] F. Beekman, F. van der Have, and B. Vastenhouw, "Sub-half mm rat brain SPECT with a dedicated ultra-high resolution focusing pinhole collimator," *J. Nucl. Med.*, vol. 49, no. Suppl 1, p. 401, 2008.

[33] B. Vastenhouw and F. J. Beekman, "Sub-mm total-body murine imaging with U-SPECT-I," *J. Nucl. Med.*, vol. 48, pp. 487–493, 2007.

[34] F. J. Beekman and F. van der Have, "The pinhole: Gateway to ultra-high resolution three-dimensional radio-nuclide imaging," *Eur. J. Nucl. Med. Mol. Imag.*, vol. 34, pp. 151–161, 2007.

[35] A. P. Jeavons, R. A. Chandler, and C. A. R. Dettmar, "A 3D HIDAC-PET camera with sub-millimetre resolution for imaging small animals," *IEEE Trans. Nucl. Sci.*, vol. 46, pp. 468–473, 1999.

[36] Y. C. Tai, A. F. Chatziioannou, Y. F. Yang, R. W. Silverman, K. Meadors, S. Siegel, D. F. Newport, J. R. Stickel, and S. R. Cherry, "MicroPET II: Design, development and initial performance of an improved microPET scanner for small-animal imaging," *Phys. Med. Biol.*, vol. 48, pp. 1519–1537, 2003.

[37] S. R. Cherry, "The 2006 Henry N. Wagner Lecture: Of mice and men (and positrons)— Advances in PET imaging technology," *J. Nucl. Med.*, vol. 47, pp. 1735–1745, Nov. 2006.

[38] F. van der Have, B. Vastenhouw, M. Rentmeester, and F. J. Beekman, "System calibration and statistical image reconstruction for ultra-high resolution stationary pinhole SPECT," *IEEE Trans. Med. Imag.*, vol. 27, pp. 960–971, 2008.

[39] J. P. W. Pluim, J. B. A. Maintz, and M. A. Viergever, "Mutual-information-based registration of medical images: A survey," *IEEE Trans. Med. Imag.*, vol. 22, pp. 986–1004, 2003.

[40] S. A. Larsson, C. Jonsson, M. Pagani, L. Johansson, and H. Jacobsson, "A novel phantom design for emission tomography enabling scatter- and attenuation-'free' single-photon emission tomography imaging," *Eur. J. Nucl. Med. Mol. Imag.*, vol. 27, pp. 131–139, Feb. 2000.

[41] K. J. Van Laere, J. Versijpt, M. Koole, S. Vandenberghe, P. Lahorte, I. Lemahieu, and R. A. Dierckx, "Experimental performance assessment of SPM for SPECT neuroactivation studies using a subresolution sandwich phantom design," *Neuroimage*, vol. 16, pp. 200–216, 2002.

[42] V. Sossi, K. R. Buckley, P. Piccioni, A. Rahmim, M. L. Camborde, E. Strome, S. Lapi, and T. J. Ruth, "Printed sources for positron emission tomography (PET)," *IEEE Trans. Nucl. Sci.*, vol. 52, pp. 114–118, 2005.

[43] T. J. Carroll, V. Teneggi, M. Jobin, L. Squassante, V. Treyer, T. F. Hany, C. Burger, L. Wang, A. Bye, G. K. von Schulthess, and A. Buck, "Absolute quantification of cerebral blood flow with magnetic resonance, reproducibility of the method, and comparison with H2(15)O positron emission tomography," *J. Cereb. Blood Flow Metab.*, vol. 22, pp. 1149–1156, Sep. 2002.

[44] M. Reivich, A. Alavi, A. Wolf, J. Fowler, J. Russell, C. Arnett, R. R. MacGregor, C. Y. Shiue, H. Atkins, A. Anand, R. Dann, and J. H. Greenberg, "Glucose metabolic rate kinetic model parameter determination in humans: The lumped constants and rate constants for [18F]fluorodeoxyglucose and [11C]deoxyglucose," *J. Cereb. Blood Flow Metab.*, vol. 5, pp. 179–192, 1985.

[45] P. Kochunov, A. E. Ramage, J. L. Lancaster, D. A. Robin, S. Narayana, T. Coyle, D. R. Royall, and P. Fox, "Loss of cerebral white matter structural integrity tracks the gray matter metabolic decline in normal aging," *Neuroimage*, vol. 45, pp. 17–28, Mar. 2009.

[46] J. Hirvonen, J. Kajander, T. Allonen, V. Oikonen, K. Någren, and J. Hietala, "Measurement of serotonin 5-HT1A receptor binding using positron emission tomography and [carbonyl-(11)C]WAY-100635-considerations on the validity of cerebellum as a reference region," *J. Cereb. Blood Flow Metab.*, vol. 27, pp. 185–195, Jan. 2007.

[47] J. Versijpt, F. Dumont, H. Thierens, H. Jansen, F. De Vos, G. Slegers, P. Santens, R. A. Dierckx, and J. Korf, "Biodistribution and dosimetry of [123I]iodo-PK 11195: A potential agent for SPET imaging of the peripheral benzodiazepine receptor," *Eur. J. Nucl. Med.*, vol. 27, pp. 1326–1333, Sep. 2000.

[48] J. C. Debruyne, J. Versijpt, K. J. van Laere, F. De Vos, J. Keppens, K. Strijckmans, E. Achten, G. Slegers, R. A. Dierckx, J. Korf, and J. L. De Reuck, "PET visualization of microglia in multiple sclerosis patients using [11C]PK11195," *Eur. J. Neurol.*, vol. 10, pp. 257–264, May 2003.

[49] M. S. Buchsbaum, B. R. Buchsbaum, E. A. Hazlett, M. M. Haznedar, R. Newmark, C. Y. Tang, and P. R. Hof, "Relative glucose metabolic rate higher in white matter in patients with schizophrenia," *Am. J. Psych.*, vol. 164, pp. 1072–1081, July 2007.

[50] M. T. Fodero-Tavoletti, C. C. Rowe, C. A. McLean, L. Leone, Q. X. Li, C. L. Masters, R. Cappai, and V. L. Villemagne, "Characterization of PiB binding to white matter in alzheimer disease and other dementias," *J. Nucl. Med.*, vol. 50, pp. 198–204, Feb. 2009.

[51] D. A. Dougherty, "Autoradiographic biological brain phantoms for emission tomography," Ph.D. dissertation, 1999.

[52] D. A. Dougherty, J. Nissanov, and G. R. Gindi, "Construction details of an autoradiographic-based rat brain phantom for emission tomography," in *Conf. Rec. IEEE Nucl. Sci. Symp. Med. Imag.*, 1998, vol. 2, pp. 1250–1254.

[53] K. C. Berridge, "The debate over dopamine's role in reward: The case for incentive salience," *Psychopharmacol. (Berl)*, vol. 191, pp. 391–431, 2007.

[54] G. Q. Chang, V. Gaysinskaya, O. Karatayev, and S. F. Leibowitz, "Maternal high-fat diet and fetal programming: Increased proliferation of hypothalamic peptide-producing neurons that increase risk for overeating and obesity," *J. Neurosci.*, vol. 28, pp. 12107–12119, Nov. 2008.

ABOUT THE AUTHORS

Frederik Johannes Beekman (Senior Member, IEEE) received the M.Sc. degree in physics from Radboud University Nijmegen, The Netherlands, in 1991 and the Ph.D degree from the University Medical Centre Utrecht, The Netherlands, in 1995.

At Delft University of Technology, he is Head of the Radiation, Detection, and Medical Imaging group. He has authored or coauthored approximately 90 peer-reviewed journal papers, several book chapters, and 20 patent applications and was presented with several international awards for his scientific contributions to SPECT technology and its application in neurosciences. His research interests include radiation technology applied to biomedical imaging (radiation detectors, SPECT, PET, transmission CTn and new (hybrid) modalities), image reconstruction from projections, and biomedical applications of SPECT, PETn and X-ray CT. He was an Associate Editor of several journals and is a Board Member of *Physics in Medicine and Biology*. He is principle Founder and part-time officer of MILabs, which develops and markets SPECT and SPECT/CT systems with an unsurpassed spatial and temporal resolution.

Brendan Vastenhouw received the master's degree in computational science and the Ph.D. degree from Utrecht University, The Netherlands, in 2001 and 2008, respectively.

During his master's study, he implemented a search engine based on latent semantic indexing, which uses a parallel supercomputer to calculate relations between words in a huge collection of documents. Beginning in 2001, he was a Scientific Programmer with the Images Sciences Institute, University Medical Center Utrecht, working on SPECT image reconstruction. He was involved in the development of the U-SPECT system and continued to work on the simulation, construction, and application of this system as a Ph.D. student. Currently, he is a part-time Postdoctoral Researcher with Delft University of Technology and part-time Programmer with MILabs.

Gijs van der Wilt received the B.Sc. degree in mechanical engineering from Hogeschool Utrecht, The Netherlands, in 1982.

From 1983 until 1992, he was with Philips, where he was involved in the development and engineering of MRI, X-ray CT, and nuclear medicine imaging devices. Since 1992, he has been the CEO/CTO of Vanderwilt Techniques, a company that designs and manufactures customized products for laboratories, research, nuclear medicine, and radiotherapy using state-of-the-art and innovative production methods.

Marcia Vervloet received the master's degree in medical computer science (medical image processing) from Utrecht University, The Netherlands, in 2003.

Since 2004, she has been with the Netherlands Institute for Health Services Research (NIVEL), Utrecht, in the research area of pharmaceutical care. In 2008, she began her Ph.D. research at NIVEL on the evaluation of the effects of an ICT-supported system (real-time medication monitoring combined with an SMS alert system) on improving adherence to oral antidiabetic medication of diabetes type-2 patients in The Netherlands.

Renée Visscher received the M.S. degree in computer science from Utrecht University, The Netherlands, in 2003.

She did a master's project in biomedical image sciences, where she contributed to the development of the rat brain phantom presented in this paper. She is currently a Consultant for ITDS, Naarden, The Netherlands.

Jan Booij was born on February 20, 1966, in The Netherlands. He graduated from Vrije Universiteit *(cum laude)*, Amsterdam, The Netherlands, in 1994 and received the Ph.D. degree from the University of Amsterdam, Amsterdam, in 1998.

His doctoral work was on dopamine transporter imaging in Parkinson's disease. Since 2002, he is registered as a Nuclear Medicine Physician. His major field of study is on neuroreceptor imaging with SPECT. He was a resident in nuclear medicine with the University of Amsterdam from 1998 to 2002. Since 2002, he has been a Nuclear Medicine Physician and Staff Member with the Department of Nuclear Medicine, University of Amsterdam. Currently, he holds a chair in experimental nuclear medicine. He is author or coauthor of more than 120 peer-reviewed publications.

Prof. Booij is a member of EANM, ECNP, IPA, and IEPA.

Mirjam Gerrits received the Ph.D. degree in 1995.

Her doctoral work was on "Initiation of Drug Addiction: The Role of Dopamine and Endogenous Opioids." In 2000, she became a Staff Member of the Rudolf Magnus Institute of Neuroscience, Department of Neuroscience and Pharmacology, University Medical Center Utrecht, The Netherlands. As an Assistant Professor, she is teaching and performing research in the fields of neuropsychopharmacology and neuroscience.

Changguo Ji received the Ph.D. degree from Peking University, Beijing, China, in 2000.

In 2001, he joined OriginLab, Northampton, MA, where he was a Scientific Programmer with data analysis and graphing. He is currently a Research Associate with the Image Sciences Institute, University Medical Center, Utrecht, The Netherlands. His current research interests include transmission and emission tomography reconstruction algorithms, image processing, medical instrumentation, and high-performance computation.

Ruud Ramakers received the bachelor's degree in applied science from the University of Utrecht, The Netherlands, in 2005.

From 2005 to 2007, he was a Research Assistant with Prof. Dr. Deutz in the Department of Surgery, Maastricht University, The Netherlands, and with the Geriatric Department, University of Arkansas Medical Sciences. He joined the Image Science Institute, The Netherlands, in December 2007 as a Research Assistant in the group of Prof. Beekman. In 2009, he joined Delft Technical University, The Netherlands.

Frans van der Have received the master's degree in applied physics from the University of Twente, Enschede, The Netherlands, in 2002 and the Ph.D. degree from Utrecht University, The Netherlands, in 2007.

In his master's research project with the Biophysical Engineering group, University of Twente, he built a fluorescence microscope into an experimental setup with magnetic tweezers for measuring the position of and forces acting on a magnetic bead in a living cell. In 2003, he joined the group of Prof. Beekman at the Image Sciences Institute, Utrecht, as a Ph.D. student, where he helped to develop the U-SPECT system. Currently, he is a Postdoctoral Researcher for Prof. Beekman with the Delft University of Technology, where he works on expanding the capabilities of U-SPECT. Since 2006, he has also been with MILabs on a part-time basis.